ADVANCED MATERIALS
www.advmat.de

Materials Views
www.MaterialsViews.com

Direct Insulation-to-Conduction Transformation of Adhesive Catecholamine for Simultaneous Increases of Electrical Conductivity and Mechanical Strength of CNT Fibers

Seongwoo Ryu, Jeffrey B. Chou, Kyueui Lee, Dongju Lee, Soon Hyung Hong, Rong Zhao, Haeshin Lee,* and Sang-gook Kim**

Over the past few decades, the fiber-based industry has achieved great progress in aerospace, military, and many other industrial applications that require light-weight materials with high mechanical strength.[1] As the demand for electronic devices has exponentially risen in recent years, the preparation of highly conductive fibers has become an important subject in the fiber industry.[2] Carbon nanotube (CNT) fibers may be an important material in advancing next-generation high-tech applications if their intrinsic mechanical,[3] electrical,[4] and thermal properties can be maintained.[5] However, due to their 1D nano-sized tubular form, it is difficult to take advantage of the outstanding properties of CNTs. Polymeric binders are widely used to strengthen CNT fibers,[6] and these binders primarily only improve the mechanical strength of the CNT fibers. However, their strength still remains far below the mechanical strength of individual CNTs due to the weak interaction between the individual CNTs in the fibers. Furthermore, the use of polymeric binders unavoidably reduces the electrical conductivity due to polymer-induced insulation and interfacial contact resistance. For example, infiltration of polyvinyl alcohol reinforces the mechanical properties of CNT fibers, which enhances the inter-nanotube load transfer and crystallinity of the polymer, but decreases the conductivity (by ≈30%) by interfering with electron transfer.[7,8] Furthermore, infiltration of a conductive polymer, such as poly(3,4-ethylenedioxythiophene) polystyrene sulfonate, has been attempted to prevent a conductivity decrease; however, it has been reported that this approach is not beneficial to the mechanical strength due to the polymer's ductile properties. Alternatively, carbonization has been studied to compensate for the electrical conductivity decrease. However, the resulting mechanical strength is far lower than that of using polymeric binders (less than 1 GPa).[9–12] Also, doping processes such as I_2,[11] H_2SO_4,[12] HSO_3Cl,[13] and $KAuBr_4$[14] could significantly improve electrical properties of CNT fibers, but their mechanical strengthening effect is insufficient. Despite previous research efforts, a method for fabricating CNT fibers with increases in both mechanical and electrical properties has not yet been developed.

This challenging task might be realized if a binder were conductive enough to not interfere with the intrinsic conductivity between the CNTs while being adequately adhesive to robustly bind the CNTs. Thus, we hypothesized that the insulation-to-conduction transformation might address the aforementioned challenge. In other words, it would be desirable to infiltrate a polymeric binder and to subsequently transform the binder into a conducting material via external stimuli, while retaining the original adhesive properties. In this work, we chose polydopamine (PDA),[15] a catecholamine polymer similar to melanin,[16] as a candidate material because it originates from the adhesive protein found in marine mussels.[17] The primary advantage of PDA is that it exhibits unparalleled adhesion to surfaces with low interfacial energy and can be converted into a conducting material via thermal treatment.[18] In fact, the principle of mussel adhesion has already been applied to carbon nanomaterials.[19] However, all previous studies on the use of adhesive binders, either PDA[20] or catecholamine materials such as poly(ethylenimine)-catechol[21], have focused only on enhancing the mechanical properties. No study has yet been published regarding a simultaneous improvement in conductivity and mechanical strength.

In this paper, we demonstrate for the first time that PDA infiltration followed by pyrolysis (i.e., the insulation-to-conduction transformation) results in increases in both the mechanical strength and conductivity of CNT fibers. We fabricated CNT fibers that exhibit both ultra-high strength (≈4000 MPa) and high electrical conductivity (≈5000 S cm^{-1}). This mechanical strength is 16 times greater than that of conventional carbon steels (≈250 MPa), and the electrical conductivity is five times

Dr. S. Ryu, Dr. J. B. Chou, Prof. S.-g. Kim
Department of Mechanical Engineering
Massachusetts Institute of Technology (MIT)
77 Massachusetts Ave., Cambridge, MA 02139, USA
E-mail: sangkim@mit.edu
K. Lee, Prof. H. Lee
Department of Chemistry
Korea Advanced Institute of Science and Technology (KAIST)
291 Daehak-ro, Daejeon 305-701, Republic of Korea
E-mail: haeshin@kaist.ac.kr
D. Lee
Korea Research Institute of Standards and Science
267 Gajeong-Ro, Yuseong-Gu, Daejeon 305-340, Republic of Korea
Prof. S. H. Hong
Department of Material Science and Engineering
Korea Advanced Institute of Science and Technology (KAIST)
291 Daehak-ro, Daejeon 305-701, Republic of Korea
Prof. R. Zhao
Engineering Product Development
Singapore University of Technology and Design (SUTD)
20 Dover Drive, Singapore 138682, Singapore
E-mail: zhao_rong@sutd.edu.sg

DOI: 10.1002/adma.201500914

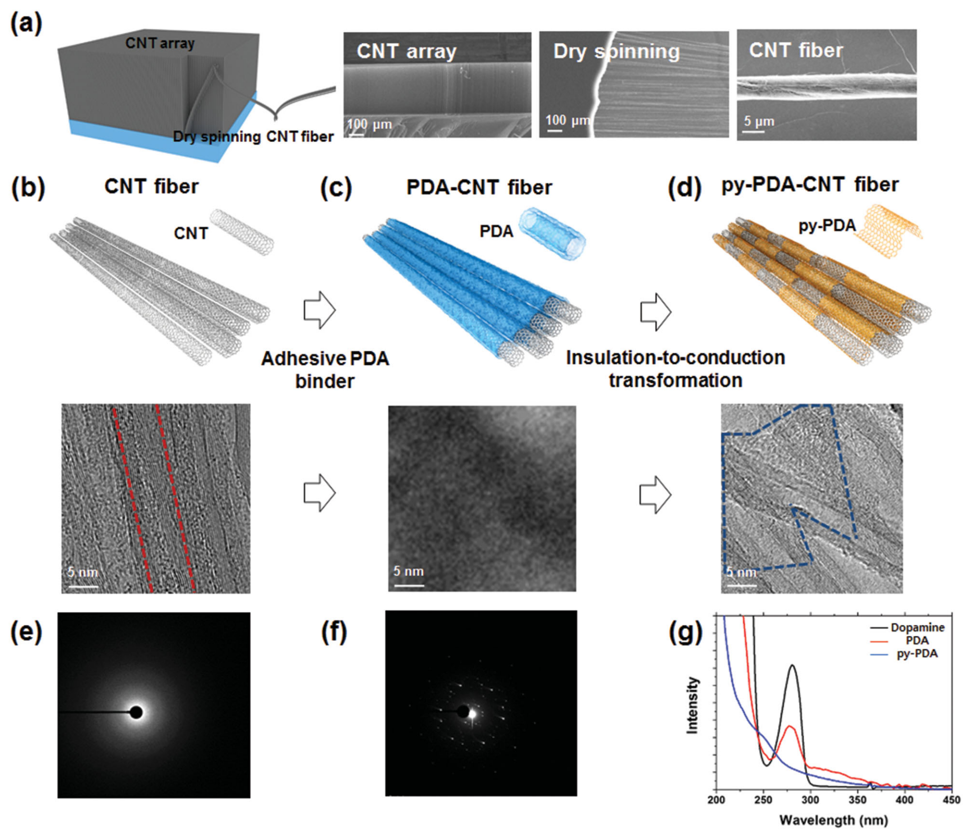

Figure 1. Fabrication process for py-PDA-CNT fibers. a) Schematic and SEM image of the dry spinning process. From left to right: SEM images of vertically aligned CNT arrays, the dry spinning process, and a py-PDA-CNT fiber. b) Schematic and TEM images of a CNT fiber (the red line represents the thickness of a single CNT), c) a PDA-CNT fiber and d) a py-PDA-CNT fiber (the blue line represents a py-PDA film). e,f) SAED pattern of PDA (e) and py-PDA (f). g) UV–vis spectra of dopamine (black), PDA (red), and py-PDA (blue).

greater than that of bulk indium tin oxide (≈1000 S cm^{-1}). The approach described herein presents a novel fabrication process that can enhance both the mechanical and electrical properties of CNT-based fibers.

We directly spun CNT fibers using a dry spinning process, which is a solid-state fiber spinning process that results in highly oriented CNT fibers. In this process, CNT fibers are directly spun from vertically aligned CNT arrays by their own van der Waals interactions.[7,22–24] The dry spinning process is considered to be easily adaptable to an industrial scale because it is similar to the method for preparing fibers from silk worms. Vertically aligned CNT arrays were synthesized on an iron (Fe) catalyst-immobilized silicon (Si) substrate by chemical vapor deposition. **Figure 1**a shows a schematic description of the on-surface synthesized CNT array and the corresponding SEM images; the heights of the CNTs were ≈290 μm. The dry spinning process was performed at a drawing rate of 10 cm min^{-1}. The vertically aligned CNT arrays were spontaneously spun by the aforementioned van der Waals interaction among neighboring CNTs, which resulted in continuous fiber spinning. The dry-spun CNT fiber underwent the following two post-treatment processes. First, a dopamine solution (2 mg of dopamine per milliliter of 10 mM tris-(hydroxymethyl) aminomethane, pH of 8.5) infiltrated the CNT fibers for 5 min (referred to as PDA-CNT fibers, Figure 1c, upper scheme). Second, the CNT fibers underwent a pyrolytic thermal conversion in a hydrogen atmosphere at 1050 °C for 2 h (Figure 1d, upper scheme). The optimized pyrolysis condition (effect of time and temperature) was shown in Figure S1 (Supporting Information). The diameter of the CNT fibers after pyrolysis was ≈7.3 μm (Figure 1a). There was no significant change in microstructure, compared with as densified CNT fiber (Figure S3, Supporting Information). After infiltration of the dopamine solution, the gaps between the CNTs were filled by oxidatively polymerized dopamine, PDA, due to the alkaline buffer condition. The insulating property of PDA resulted in non-clear, noisy images of the PDA-CNT fibers (Figure 1c, bottom). However, after pyrolysis, clear images of the py-PDA-CNT fibers were obtained. Additionally, we found small portions of py-PDA (i.e., pyrolyzed PDA) films that were wrapped around the surfaces of the CNT fibers and interconnected between the fibers (Figure 1d, dotted line, bottom). The structures of the PDA- and py-PDA-CNT fibers were further analyzed using selected area electron diffraction (SAED). Before pyrolysis, a diffraction ring was observed, as shown in Figure 1e. After pyrolysis, the previous diffraction ring had primarily disappeared, and a hexagonal diffraction pattern was observed (Figure 1f). The SAED results demonstrate that the amorphous polymeric structure was thermally converted to a multilayer graphene-like structure. This property conversion is novel in that the one-step thermal treatment resulted in:

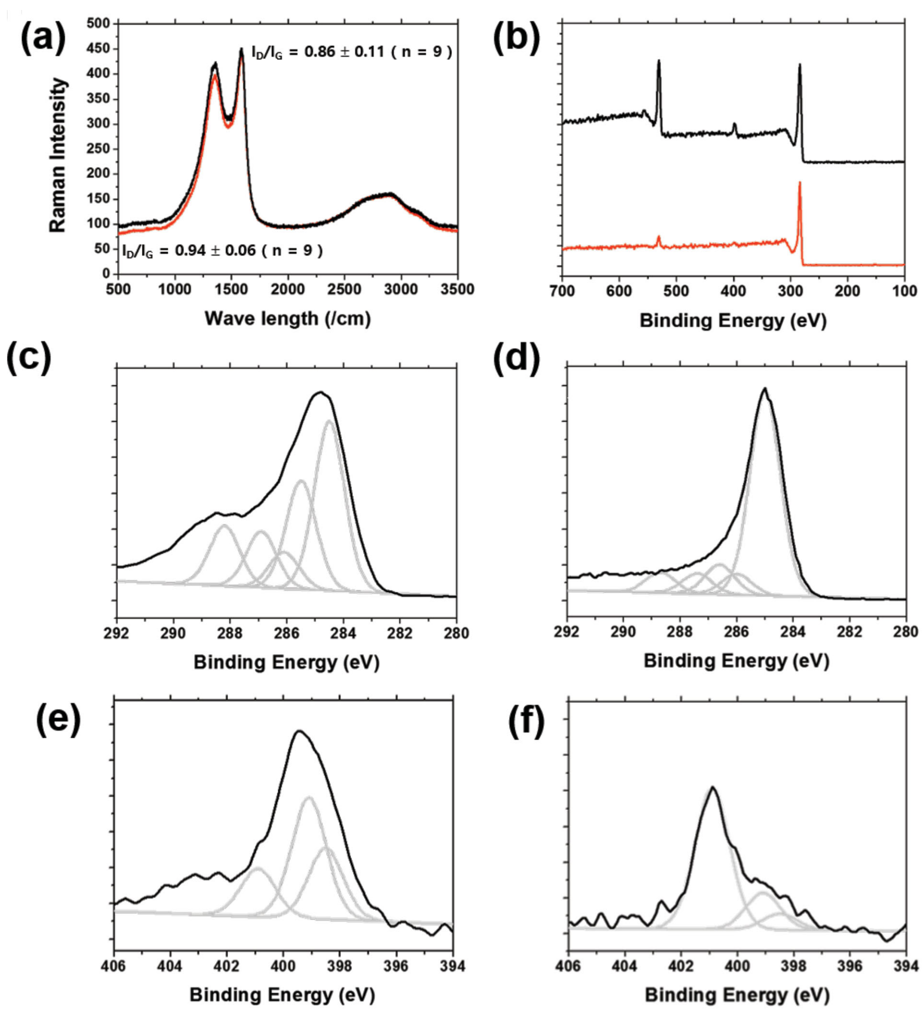

Figure 2. Analysis of the chemical composition of a CNT fiber. a) Raman spectra of the D- and G-bands of PDA (black) and py-PDA (red). b) XPS spectra of PDA (black) and py-PDA (red). XPS analysis reveals a peak corresponding to C1s at 284.5 eV (PDA: 73.96%, py-PDA: 91.77%), N1s at 401.1 (PDA: 4.32%, py-PDA: 1.81%) and O1s at 532.1 eV (PDA: 21.72%, py-PDA: 6.41%). c,d) High-resolution XPS narrow scans of the C1s region of PDA (c) and py-PDA (d). The C1s peak reveals C—C at 284.5 eV, C—OH at 285.5 eV, C—N sp^2 at 286.1 eV, C—O—C at 286.8 eV, and C—N sp^3 at 288.2 eV. e,f) High-resolution XPS narrow scans of the N1s region of PDA (e) and py-PDA (f). N1s peak reveals graphitic N at 400.9 eV, pyrrolic N at 399.0 eV, and pyridinic N at 398.4 eV.

i) an insulation-to-conduction transformation of the PDA and ii) maintenance of the intrinsic adhesive property of the PDA. This graphene-like structure was also indicated by X-ray diffraction (XRD) analysis (Figure S2, Supporting Information). After pyrolysis, a broad peak appeared between 2θ values of 21.7 and 24.8°. The corresponding d-spacing was ≈0.4 nm for py-PDA. This result reflects the existence of an ordered packed structure that includes an (002) region of graphite.[25] To verify the self-polymerization and thermal conversion after pyrolysis, UV–vis spectra were obtained from the PDA and py-PDA dispersed solutions (Figure 1g). Compared to the dopamine spectrum, the PDA exhibited a broad peak at 320 nm with a decreased unoxidized catechol peak at 280 nm, which indicates oxidative self-polymerization of dopamine.[26] After pyrolysis, the unoxidized catechol peak had essentially disappeared, and an absorption peak was observed at 238 nm, which corresponds to the π–π* transition.[27]

The py-PDA's graphitic nature was further analyzed by Raman and X-ray photoelectron spectroscopy (XPS). Raman spectroscopy was used to characterize the vibrational modes of the PDA and py-PDA (**Figure 2**a). The Raman spectra of both PDA and py-PDA displayed a D-band at 1350 cm^{-1} and a broad G-band at 1590 cm^{-1}. The I_D/I_G ratio of the PDA was 0.94 ± 0.06 (n = 9), which decreased to 0.86 ± 0.11 (n = 9) after pyrolysis. The decreased I_D/I_G ratio indicates that the dominant G peak in the py-PDA corresponds to the thermal production of graphitic carbon after pyrolysis.[28] XPS was used to analyze the chemical composition of the PDA and py-PDA. The peaks at 284.5, 401.1, and 532.1 eV correspond to C1s, N1s, and O1s in the PDA and py-PDA (Figure 2b). After pyrolysis, a significant decrease in the N1s and O1s peaks was observed due to chemical reduction and graphitization. High-resolution C1s and N1s spectra from the py-PDA revealed significant differences in the carbon chemistry of the PDA. The high-resolution

C1s spectra indicated the presence of C—C bonding at 284.5 eV, C—O bonding at 285.5 eV, C—N sp^2 bonding at 286.1 eV, C—O—C bonding at 286.8 eV, and C—N sp^3 bonding at 288.2 eV (Figure 2c,d). The C—C level increased significantly after pyrolysis, from 39.28% (PDA) to 68.94% (py-PDA). Moreover, the level of C—N sp^2 bonding slightly increased from 8.49% (PDA) to 10.1% (py-PDA), and the C—N sp^3 bonding decreased from 13.96% (PDA) to 6.97% (py-PDA). The high-resolution N1s spectra exhibited similar shifts after pyrolysis. The high-resolution N1s spectra indicated the presence of graphitic N at 400.9 eV, pyrrolic N at 399.0 eV, and pyridinic N at 398.4 eV (Figure 2e,f). The major N1s peak observed in the PDA corresponded to pyrrolic N (50.31%), whereas the N1s peak observed in the py-PDA corresponded to graphitic N (72.53%). This result is consistent with the SAED and Raman characterization of the graphitic structure of py-PDA after pyrolysis. From this structural transformation, we conclude that py-PDA has a structure analogous to nitrogen-doped multilayer graphitic planes.[29]

Therefore, the py-PDA conversion from PDA is novel because the infiltrated PDA plays a role as an adhesive polymer, which increases the inter-CNT binding strength, and is later converted to a conductive, graphitic py-PDA adhesive by pyrolysis. As expected, we observed that all three important mechanical properties, i.e., tensile strength, elongation, and fiber modulus, increased upon py-PDA conversion. **Figure 3**a shows the tensile strength of as-drawn CNT, PDA-CNT, and py-PDA-CNT fibers. After pyrolysis, the tensile strength of the py-PDA increased, with values of 1004 ± 184 MPa (n = 9) for the CNT fibers and 4035 ± 549 MPa (n = 9) for the py-PDA-CNT fibers. Furthermore, both the fiber modulus and maximum elongation increased after pyrolysis. The modulus was calculated to be 83.33 ± 8.53 GPa (n = 9) for the py-PDA-CNT fibers and 29.41 ± 3.53 GPa (n = 9) for the CNT fibers. The elongation exhibited about 77% increase from 3.39 ± 0.36 (n = 9) for the CNT fibers and 6.01 ± 0.82 (n = 9) for the py-PDA-CNT fibers. As a result, compared to the initial CNT fibers, the py-PDA-CNT fiber exhibited remarkable increased tensile strength (402%), modulus (286%), and elongation (177%). Therefore, py-PDA plays an unprecedented role in the adhesive ability among CNTs, in which the primary bonding mechanism may be based on π–π interactions generated by pyrolysis. Moreover, we observed sudden, small drops in the strength–elongation curve during py-PDA-CNT fiber extension, as indicated by the arrows. This discontinuous behavior indicates partial mechanical failure driven by slippage or breaking between py-PDA and CNT.[30] This failure usually accelerates stress concentration at the defect sites or mechanical cracks until eventual full failure. However, in the py-PDA-CNT fiber, load transfer was continuously carried out by the physicochemical hybrid of py-PDA and CNT. Before the pyrolysis process, the PDA infiltration produced a negative effect on both the tensile strength and maximum elongation of the PDA-CNT fibers: 732 ± 311 MPa (n = 9) for strength and 1.41 ± 0.21% (n = 9) for maximum elongation. The only positive result for the PDA infiltration was a slight increase in the modulus from 29.41 ± 3.53 GPa to 54.04 ± 3.53 GPa (n = 9)). Due to intrinsic adhesive properties, the PDA fiber exhibited an improved modulus. However, modulus enhancement of PDA-CNT fiber (183%) is still below enhancement of py-PDA-CNT fiber (283%). This result indicates that the catechol and/or 5,6-hydroxyindole in the non-pyrolyzed PDA exhibit intrinsic adhesive properties but are not as effective as the py-PDA. The TEM fractography results shown in Figure 3b provide an insight into the mechanical strengthening effect. Typical hairy-type failure between individual CNTs was

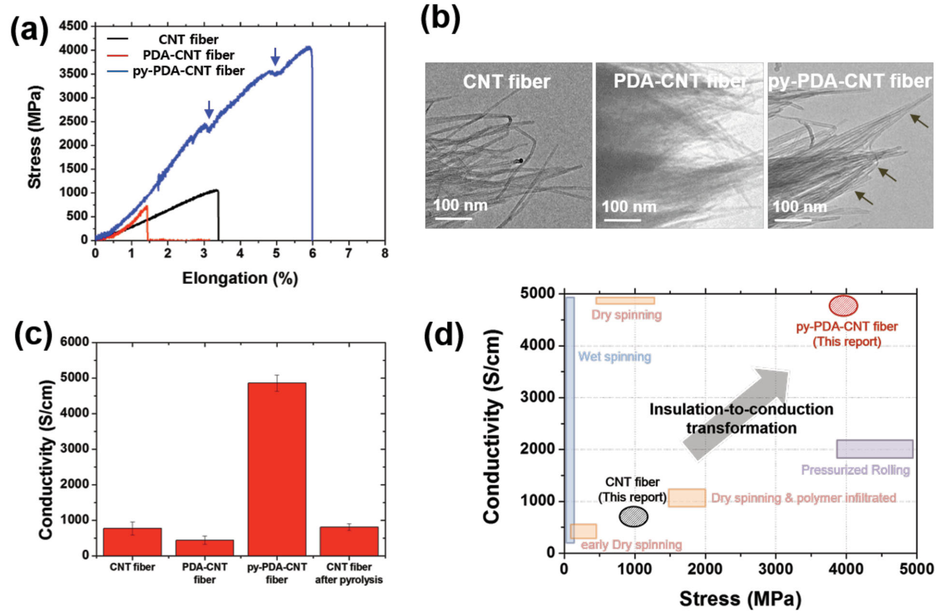

Figure 3. Mechanical and electrical properties of a CNT fiber. a) Force–distance curves for an as-drawn CNT fiber (control) (black), PDA-CNT fiber (red), and py-PDA-CNT fiber (blue). b) TEM fractography images of a CNT fiber, PDA-CNT fiber, and py-PDA-CNT fiber (the grey arrow represents a py-PDA film). c) Electrical conductivity of a CNT fiber, PDA-CNT fiber, py-PDA-CNT fiber, and CNT fiber after pyrolysis. d) Comparison of the strength and electrical conductivity of the py-PDA-CNT fiber and previously reported CNT-based fibers produced via wet spinning,[10,36,37] dry spinning,[7,38] polymer-infiltrated dry spinning,[8] and pressurized rolling.[39]

observed in the non-PDA-treated CNT fibers. CNT fiber failure is typically driven by a stress concentration at a void and/or at the end point of the CNTs, where interactions between CNTs are weak. Therefore, the polymer infiltration technique typically fills voids and improves the inter-nanotube load transfer.[31] After PDA infiltration, a cloud-like, coated PDA layer was observed; however, the brittle fractures indicate that an effective load transfer was not achieved in the PDA-CNT fibers. We can assume that the interaction between the PDA and the CNTs is not as strong as the interaction between individual CNTs.[32] However, the fractography of the py-PDA-CNT fibers shows a typical carbon composite material in which a thin graphitic film of py-PDA is interconnected between the CNTs (Figure 3b, grey arrow). As a result, the strong graphitic interaction and the additional interaction area for the py-PDA and CNTs lead to an effective load transfer, resulting in strong mechanical strength.

In general, infiltration of organic polymers results in decreased conductivity. For example, previous attempts of applying polymeric post-treatments to enhance mechanical properties have resulted in the creation of insulating regions within the CNT fibers.[33] However, the conversion from PDA to py-PDA does not sacrifice the electrical properties of the CNT fibers, while still maintaining the role of a binder between the CNTs. Figure 3c shows the electrical conductivity for the CNT, PDA-CNT, and py-PDA-CNT fibers. Simple PDA infiltration resulted in a conductivity decrease from 772 ± 186 (n = 9) to 442.5 ± 115 S cm^{-1} (n = 9), followed by a significant increase to 4856 ± 223 S cm^{-1} (n = 9) after pyrolysis. This result is due to the graphitic conversion observed in PDA, in which the graphitic py-PDA is structurally similar to nitrogen-doped graphene.[29] As an important control, the pyrolysis itself without PDA resulted in only a slight conductivity increase. As-drawn CNT fibers without PDA infiltration were subjected to the same pyrolytic conditions. However, the CNT fibers after pyrolysis exhibited only a slight increase in conductivity to 810 ± 92 S cm^{-1} (n = 9), which might be due to additional graphitization. This result indicates that the conductivity enhancement observed in the py-PDA-CNT fibers is not due to thermal conversion of the CNTs. The conductivity of a CNT fiber is a function of the contact resistance between the nanotubes, which strongly depends on the contact area and intertube spacing.[34,35] The infiltrated PDA layer in the CNT fiber (PDA-CNT) is initially an insulator, which largely attenuates the electrical tunneling effect between CNTs. However, once the PDA is converted into graphitic py-PDA after pyrolysis, the newly generated graphitic features of the py-PDA recover the previously lost conductive paths, as demonstrated in Figure 1f. Finally, to further emphasize the results described herein, Figure 3d provides a comparison of the mechanical strength and electrical conductivity for previously reported CNT fibers obtained via wet spinning,[10,36,37] dry spinning,[7,38] polymer-infiltrated dry spinning,[8] and pressurized rolling.[39]. None of these techniques increased both the mechanical and electrical properties to a satisfactory level. Dry spinning of CNTs resulted in good electrical conductivity but led to poor mechanical strength. In contrast, pressurized rolling largely increased the mechanical properties but only marginally increased the conductivity. Thus, the method described herein for preparing py-PDA-CNT fibers presents a good alternative solution for future carbon nanomaterial science and engineering.

In conclusion, we report a completely new function of PDA for carbon material preparation by pyrolysis based on the insulation-to-conduction transformation from PDA to py-PDA. By maintaining the intrinsic, material-independent adhesive functions of PDA, infiltrated PDA effectively binds onto the surface of the CNTs in a fiber. Later, pyrolysis converts the PDA into py-PDA, which acts a conductive adhesive polymer that enhances both the mechanical properties and the conductivity. The property conversion of PDA is novel, considering that previous attempts to use polymers (i.e., binders) to increase the mechanical strength of CNT fibers unavoidably decreased the conductivity. The mechanical strength of py-PDA-infiltrated CNT fibers exhibits a remarkable increase of ≈400% combined with an ≈630% enhancement in conductivity. This result opens a new research direction for PDA, which could be a useful adhesive polymer for carbon nanomaterials and related composite fabrications.

Supporting Information

Supporting Information is available from the Wiley Online Library or from the author.

Acknowledgements

This work was supported by the SUTD-MIT Postdoctoral Program.

Received: February 23, 2015
Revised: March 21, 2015
Published online: April 20, 2015

[1] J. W. S. Hearle, *High-Performance Fibres*, Woodhead Publishing, Cambridge, UK **2001**, pp. 2–16.
[2] L. M. Castano, A. B. Flatau, *Smart Mater. Struct.* **2014**, *23*, 1
[3] M. F. Yu, O. Lourie, M. J. Dyer, K. Moloni, T. F. Kelly, R. S. Ruoff, *Science* **2000**, *287*, 637.
[4] A. Javey, J. Gue, Q. Wang, M. Lundstrom, H. Dai, *Nature* **2003**, *424*, 654.
[5] M. F. Yu, B. S. Files, S. Arepalli, R. S. Ruoff, *Phys. Rev. Lett.* **2000**, *84*, 5552.
[6] N. Behabtu, M. J. Green, M. Pasquali, *Nano Today* **2008**, *3*, 24.
[7] M. Zhang, K. R. Atkinson, R. H. Baughman, *Science* **2004**, *306*, 1358.
[8] K. Liu, Y. H. Sun, X. Y. Lin, R. F. Zhou, J. P. Wang, S. S. Fan, K. L. Jiang, *ACS Nano* **2010**, *4*, 5827.
[9] S. Badaire, V. Pichot, C. Zakri, P. Poulin, P. Launois, J. Vavro, C. Guthy, M. Chen, J. E. Fischer, *J. Appl. Phys.* **2004**, *96*, 7509.
[10] M. E. Kozlo, R. C Capps, W. M. Sampson, V. H. Ebron, J. P. Ferraris, R. H. Baughman, *Adv. Mater.* **2005**, *17*, 614.
[11] Y. Zhao, J. Wei, R. Vajtai, P. M. Ajayan, E. V. Barrera, *Sci. Rep.* **2011**, *1*, 83.
[12] L. M. Ericson, H. Fan, H. Peng, V. A. Davis, W. Zhou, J. Sulpizio, Y. Wang, R. Booker, J. Vavro, C. Guthy, A. N. G. Parra-Vasquez, M. J. Kim, S. Ramesh, R. K. Saini, C. Kittrell, G. Lavin, H. Schmidt, W. W. Adams, W. E. Billups, M. Pasquali, W.-F. Hwang, R. H. Hauge, J. E. Fischer, R. E. Smalley, *Science* **2004**, *305*, 1447.
[13] N. Behabtu, C. C. Young, D. E. Tsentalovich, O. Kleinerman, X. Wang, A. W. K. Ma, E. A. Bengio, R. F. ter Waarbeek, J. J. de Jong,

R. E. Hoogerwerf, S. B. Fairchild, J. B. Ferguson, B. Maruyama, J. Kono, Y. Talmon, Y. Cohen, M. J. Otto, M. Pasquali, *Science* **2013**, *339*, 182.
[14] J. Alvarenga, P. R. Jarosz, C. M. Schauerman, B. T. Moses, B. J. Landi, C. D. Cress, R. P. Raffaelle, *Appl. Phys. Lett.* **2010**, *97*, 182106.
[15] H. Lee, S. M. Dellatore, W. M. Miller, P. B. Messersmith, *Science* **2007**, *318*, 426.
[16] M. d'Ischia, A. Napolitano, A. Pezzella, P. Meredith, T. Sarna, *Angew. Chem.* **2009**, *121*, 3972.
[17] J. H. Waite, X. Qin, *Biochemistry* **2001**, *49*, 2887.
[18] J. Kong, W. A. Yee, L. Yang, Y. Wei, S. L. Phua, H. G. Ong, J. M. Ang, X. Li, X. Lu, *Chem. Commun.* **2012**, *48*, 10316.
[19] H. Hu, B. Yu, Q. Ye, Y. Gu, F. Feng, *Carbon* **2010**, *48*, 2347.
[20] S. H. Hwang, D. Kang, R. S. Ruoff, H. S. Shin, Y. B. Park, *ACS Nano* **2014**, *7*, 6739.
[21] S. Ryu, Y. Lee, J. W. Hwang, S. Hong, C. Kim, T. G. Park, H. Lee, S. H. Hong, *Adv. Mater.* **2011**, *17*, 1971.
[22] X. Zhang, K. Jiang, C. Feng, P. Liu, L. Zhang, J. Kong, T. Zhang, Q. Li, S. Fan, *Adv. Mater.* **2006**, *18*, 1505.
[23] X. Zhang, Q. Li, T. G. Holesinger, P. N. Arendt, J. Huang, P. D. Kirven, T. G. Clapp, R. F. DePaula, X. Liao, Y. Zhao, L. Zheng, D. E. Petereson, Y. Zhu, *Adv. Mater.* **2007**, *19*, 4198.
[24] X. Zhang, Q. Li, Y. Tu, Y. Li, J. Y. Coulter, L. Zheng, Y. Zhao, Q. Jia, D. E. Peterson, Y. Zhu, *Small* **2007**, *2*, 244.
[25] B. E. Warren, *Phys. Rev.* **1941**, *59*, 693.
[26] B. P. Lee, J. L. Dalsin, P. B. Messersmith, *Biomacromolecules* **2002**, *3*, 1038.
[27] D. Pan, J. Zhang, M. Wu, *Adv. Mater* **2010**, *22*, 734.
[28] A. C. Ferrari, J. C. Meyer, V. Scardaci, C. Casiraghi, M. Lazzeri, F. Mauri, S. Piscanec, D. Jiang, K. S. Novoselov, S. Roth, A. K. Geim, *Phys. Rev. Lett.* **2006**, *97*, 187401.
[29] J. Kong, W. A. Yee, Y. Wei, L. Yang, J. M. Ang, S. L. Phua, S. Y. Wong, R. Zhou, Y. Dong, X. Li, X. Lu, *Nanoscale* **2013**, *5*, 2967.
[30] H. Hu, B. Yu, Q. Ye, Y. Gu, F. Feng, *Carbon* **2012**, *50*, 4175.
[31] Y. Liu, S. Kumar, *ACS Appl. Mater. Interfaces* **2014**, *6*, 6069.
[32] A. Rochefort, J. D. Wuest, *Langmuir* **2009**, *25*, 210.
[33] W. Lu, M. Zu, J. H. Byun, T. W. Chu, *Adv. Mater.* **2012**, *24*, 1805–1833.
[34] M. B. Jakubinek, J. B. Johnson, M. A. White, C. Jayasinghe, G. Li, W. D. Cho, M. J. Schulz, V. Shanov, *Carbon* **2012**, *50*, 244.
[35] M. H. Miao, *Carbon* **2011**, *49*, 3755.
[36] L. M. Ericson, H. Fan, H. Q. Peng, V. A. Davis, W. Zhou, J. Sulpizio, Y. H. Wang, R. Booker, J. Vavro, C. Guthy, A. N. G. Parra-Vasquez, M. J. Kim, S. Ramesh, R. K. Saini, C. Kittrell, G. Lavin, H. Schmidt, W. W. Adams, W. E. Billups, M. Pasquali, W. F. Hwang, R. H. Hauge, J. E. Fischer, R. H. Smalley, *Science* **2004**, *305*, 1447.
[37] V. A. Davis, A. N. G. Parra-Vasquez, M. J. Green, P. K. Rai, N. Behabtu, V. Prieto, R. D. Booker, J. Schmidt, E. Kesselman, W. Zhou, H. Fan, W. W. Adams, R. H. Hauge, J. E. Fischer, Y. Cohen, Y. Talmon, R. E. Smalley, M. Pasquali, *Nat. Nanotechnol.* **2009**, *4*, 830.
[38] X. H. Zhong, Y. L. Li, Y. K. Liu, Y. Feng, J. Liang, J. Jin, L. Zhu, F. Hou, J. Y. Li, *Adv. Mater.* **2010**, *22*, 692.
[39] J. N. Wang, X. G. Luo, T. Wu, Y. Chen, *Nat. Commun.* **2014**, *5*, 3848.